

Mean-field descriptions of collective migration with strong adhesion

Stuart T. Johnston,¹ Matthew J. Simpson,^{1,2} and Ruth E. Baker³

¹*School of Mathematical Sciences, Queensland University of Technology, Brisbane, Australia*

²*Tissue Repair and Regeneration Program, Institute of Health and Biomedical Innovation (IHBI), Queensland University of Technology, Brisbane, Australia*

³*Centre for Mathematical Biology, Mathematical Institute, University of Oxford, 24-29 St Giles', Oxford OX1 3LB, United Kingdom*

(Received 21 March 2012; revised manuscript received 11 May 2012; published xxxxx)

Random walk models based on an exclusion process with contact effects are often used to represent collective migration where individual agents are affected by agent-to-agent adhesion. Traditional mean-field representations of these processes take the form of a nonlinear diffusion equation which, for strong adhesion, does not predict the averaged discrete behavior. We propose an alternative suite of mean-field representations, showing that collective migration with strong adhesion can be accurately represented using a moment closure approach.

DOI: [10.1103/PhysRevE.00.001900](https://doi.org/10.1103/PhysRevE.00.001900)

PACS number(s): 87.17.Rt, 87.17.Jj

I. INTRODUCTION

Microscopic transport processes modulated by adhesion are important for many applications including the study of biomolecules [1], granular media [2], and biological cells [3,4]. For these applications it is essential to understand how individual-level details of the adhesion mechanism lead to population-level properties that govern system-wide behavior. Therefore, accurate mean-field models of these mechanisms are essential. Here, we study a discrete motility mechanism based on an exclusion process [5] with contact effects. These models have been used to study the migration of glioma cells [6,7], breast cancer cells [8], and wound healing processes [9]. Anguige and Schmießer [10] were the first to derive a mean-field description of such a discrete model, with others reported subsequently [6,8,11,12]. These previous studies reported mean-field representations in the form of a nonlinear diffusion partial differential equation (pde) [12].

The form of the nonlinear diffusivity function reflects the physical behavior in the discrete model [10–12]. When contact enhances migration, the nonlinear diffusivity function is always positive [6,11,13,14]. When contacts reduce migration (i.e., adhesion), the nonlinear diffusivity function can become negative when contact effects dominate [8,10,11]. The transition from positive to negative nonlinear diffusivity is associated with clustering in the discrete simulations [13]; under these conditions existing mean-field models do not predict the average behavior of the discrete process [6,11,13]. For example, both Deroulers *et al.* [6] and Fernando *et al.* [11] showed that the traditional mean-field pde fails to make accurate predictions when contact effects became sufficiently strong. Fernando *et al.* [11] provided further insight by proposing a heuristic measure to predict the parameter regime where the mean-field pde was either accurate or inaccurate. Although insightful, this previous study provided no means of making accurate mean-field predictions when contact effects were strong.

Currently, it is impossible to quantify how and why the traditional pde representation fails to predict the averaged discrete behavior as these models provide no way of examining the validity of the assumptions underlying the traditional mean-field pde. Here we address these issues by showing that an adhesive motility mechanism can be described by a suite

of three mean-field models. We show that the traditional pde invokes two key assumptions, namely,

(1) that effects of $\mathcal{O}(\Delta^3)$ and smaller are neglected in the limit that $\Delta \rightarrow 0$, where Δ is the lattice spacing, and

(2) that the occupancy status of lattice sites are assumed to be independent so that correlation effects are ignored.

Two alternative mean-field models are developed that relax both these assumptions independently. Comparing averaged discrete simulation results to the predictions of the suite of three mean-field models highlights the role of correlation effects and shows that it is possible to make accurate mean-field predictions with strong adhesion using a moment closure approach.

II. DISCRETE MECHANISM

We consider a one-dimensional lattice, with spacing Δ . Sites are indexed by l , and have location $x = l\Delta$. Time is uniformly discretized with time step τ , and a random sequential update method is used to simulate the process [15]. During each time step, agents attempt to step to nearest neighbor sites provided that the target site is vacant. Motility events that would place an agent on an occupied site are aborted. Motility events are regulated by contact effects that represent agent-to-agent adhesion [10] by altering the motility using an adhesion parameter $\sigma \in [-1, 1]$. For example, if we consider the schematic illustration in Fig. 1, the agent at site $l - 1$ would attempt to move to the vacant site $l - 2$ with probability $(1 - \sigma)/2$ per time step when site l is occupied. Alternatively, this event would occur with probability $1/2$ per time step if site l were vacant. Setting $\sigma > 0$ represents adhesion, whereas setting $\sigma < 0$ represents repulsion [11].

III. MEAN-FIELD REPRESENTATIONS

We define the lattice variable, $\phi_l \in \{0_l, C_l\}$, to represent the state of the l th site, so that $\phi_l = 0_l$ indicates that site l is vacant and $\phi_l = C_l$ indicates that site l is occupied. Averaging the occupancy of each site over many identically prepared realizations gives $c_l \in [0, 1]$ [6,11]. In our notation upper case C_l represents the occupancy of the l th site in a single realization, whereas lower case c_l represents the average occupancy, where the average is constructed over a

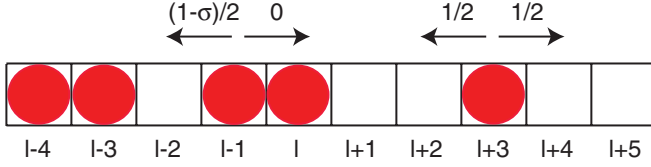


FIG. 1. (Color online) The random walk takes place on a one-dimensional lattice where each site can be occupied, at most, one agent. An isolated agent steps in the positive or negative x direction with probability $1/2$ per computational time step. For example, the agent at site $l+3$ would step to site $l+2$ with probability $1/2$, or to $l+4$ with probability $1/2$. Contact effects alter the motility probability; for example, in the configuration shown, the agent at site $l-1$ would step to $l-2$ with probability $(1-\sigma)/2$, where $\sigma \in [-1,1]$ represents the contact effect. The agent at site $l-1$ would step to site l with probability 0 since the target site is occupied.

large number of identically prepared realizations of the same process. We now introduce three ways to approximate c_l by making different assumptions about the underlying discrete process.

A. Partial differential equation representation

To connect the discrete mechanism with a pde, we form a discrete conservation statement describing δc_l , the change in average occupancy of site l per time step. The conservation equation can be written as

$$\begin{aligned} \delta c_l = & \frac{1}{2}[c_{l-1}(1-c_l)(1-\sigma c_{l-2}) + c_{l+1}(1-c_l)(1-\sigma c_{l+2})] \\ & - \frac{1}{2}[c_l(1-c_{l-1})(1-\sigma c_{l+1}) \\ & + c_l(1-c_{l+1})(1-\sigma c_{l-1})], \end{aligned} \quad (1)$$

where positive terms on the right of Eq. (1) represent events that would place agents at site l , and negative terms represent events that would remove agents from site l . The discrete conservation statement is related to a pde as $\Delta \rightarrow 0$ and $\tau \rightarrow 0$, and c_l is identified as a continuous variable $c(x,t)$ [6,10,11]. Expanding all terms in Eq. (1) in a truncated Taylor series about site l , neglecting terms of $\mathcal{O}(\Delta^3)$ and higher [6,10,11], and dividing the resulting expression by τ , we take limits as $\Delta \rightarrow 0$ and $\tau \rightarrow 0$ with the ratio (Δ^2/τ) held constant [16] to obtain

$$\frac{\partial c}{\partial t} = D_0 \frac{\partial}{\partial x} \left[D(c) \frac{\partial c}{\partial x} \right], \quad (2)$$

where $D_0 = \lim_{\Delta, \tau \rightarrow 0} (\Delta^2)/(2\tau)$ is the free-agent diffusivity, and the nonlinear diffusivity function is given by [10,11]

$$D(c) = 1 - \sigma c(4 - 3c). \quad (3)$$

Two key assumptions lead to Eq. (2). First, we assume terms of $\mathcal{O}(\Delta^3)$ and smaller can be neglected. Second, we assume the average occupancies of sites to be independent so that, for example, the net averaged probability of a transition from site l to $l+1$ is proportional to $(1-c_{l+1})(1-\sigma c_{l-1})$. This implies that the occupancy of sites $l+1$ and $l-1$ are independent, which, in general, is untrue [17,18]. Without further analysis, it is impossible to deduce how these two assumptions control the net error associated with Eq. (2). We now introduce two alternative mean-field models that systematically relax both assumptions.

B. Ordinary differential equation representation

To avoid neglecting terms of $\mathcal{O}(\Delta^3)$ and smaller as $\Delta \rightarrow 0$, we retain the spatial structure of the random walk in Eq. (1) by identifying discrete values of c_l with a continuous variable $c_l(t)$. Dividing Eq. (1) by τ , and considering the limit as $\tau \rightarrow 0$, gives a system of ordinary differential equations (odes)

$$\begin{aligned} \frac{dc_l}{dt} = & \frac{1}{2}[c_{l-1}(1-c_l)(1-\sigma c_{l-2}) + c_{l+1}(1-c_l)(1-\sigma c_{l+2})] \\ & - \frac{1}{2}[c_l(1-c_{l-1})(1-\sigma c_{l+1}) + c_l(1-c_{l+1})(1-\sigma c_{l-1})], \end{aligned} \quad (4)$$

for each site l . We note that Eq. (4) still makes the independence assumption, and we now develop a third mean-field model that removes this assumption.

C. Moment closure representation

We use k -point distribution functions, $\rho^{(k)}$ ($k = 1, 2, 3, \dots$), to describe the averaged occupancies of k tuples of lattice sites [17,19,20]. For $k = 1$, the distribution function is a univariate distribution describing the average density of agents on site l so that $\rho^{(1)}(C_l) = c_l$. For $k = 2$, the bivariate distribution function can be defined in terms of correlation functions [17,19], which can be written as

$$F(l,m) = \frac{\rho^{(2)}(C_l, C_m)}{\rho^{(1)}(C_l)\rho^{(1)}(C_m)}, \quad (5)$$

where $l \neq m$. These correlation functions allow us to relax the independence assumptions inherent in Eqs. (2) and (4). Setting $F(l,m) \equiv 1$ indicates that the occupancies of sites l and m are independent. Instead, we avoid this assumption by allowing $F(l,m)$ to evolve as part of the solution [17]. With these definitions we have

$$\begin{aligned} \frac{dc_l}{dt} = & \frac{1}{2}[\rho^{(3)}(0_{l-2}, C_{l-1}, 0_l) + (1-\sigma)\rho^{(3)}(C_{l-2}, C_{l-1}, 0_l)] \\ & + \frac{1}{2}[\rho^{(3)}(0_l, C_{l+1}, 0_{l+2}) + (1-\sigma)\rho^{(3)}(0_l, C_{l+1}, C_{l+2})] \\ & - \frac{1}{2}[\rho^{(3)}(0_{l-1}, C_l, 0_{l+1}) - (1-\sigma)\rho^{(3)}(0_{l-1}, C_l, C_{l+1})] \\ & - \frac{1}{2}[\rho^{(3)}(0_{l-1}, C_l, 0_{l+1}) - (1-\sigma)\rho^{(3)}(C_{l-1}, C_l, 0_{l+1})]. \end{aligned} \quad (6)$$

Positive terms on the right of Eq. (6) represent events that would place an agent at site l whereas negative terms on the right of Eq. (6) represent events that would remove an agent from site l . To simplify Eq. (6) we apply a summation rule [17] to rewrite the unbiased $\rho^{(3)}$ terms as equivalent $\rho^{(2)}$ terms. The Kirkwood superposition approximation (KSA) is then used to rewrite the remaining $\rho^{(3)}$ terms as combinations of $\rho^{(2)}$ terms. The KSA is a moment closure approximation that has been used in many applications, including ecology [21–23], physical chemistry [24], disease biology [25,26], and diffusion-mediated reactions [27]. The KSA can be written as

$$\rho^{(3)}(\phi_l, \phi_m, \phi_n) = \frac{\rho^{(2)}(\phi_l, \phi_m)\rho^{(2)}(\phi_l, \phi_n)\rho^{(2)}(\phi_m, \phi_n)}{\rho^{(1)}(\phi_l)\rho^{(1)}(\phi_m)\rho^{(1)}(\phi_n)}. \quad (7)$$

161 Combining Eq. (7) with the simplified version of Eq. (6) gives

$$\begin{aligned} \frac{dc_l}{dt} = & \frac{1}{2}[c_{l+1} - 2c_l + c_{l-1}] - \frac{\sigma}{2(1-c_l)}\{c_{l-2}c_{l-1}[1 - c_l F(l-2, l)][1 - c_l F(l-1, l)]F(l-2, l-1)\} \\ & - \frac{\sigma}{2(1-c_l)}\{c_{l+1}c_{l+2}[1 - c_l F(l, l+1)][1 - c_l F(l, l+2)]F(l+1, l+2)\} + \frac{\sigma}{2(1-c_{l-1})}\{c_l c_{l+1}[1 - c_{l-1} F(l-1, l)] \\ & \times [1 - c_{l-1} F(l-1, l+1)]F(l, l+1)\} + \frac{\sigma}{2(1-c_{l+1})}\{c_{l-1}c_l[1 - c_{l+1} F(l-1, l+1)][1 - c_{l+1} F(l, l+1)]F(l, l-1)\}. \end{aligned} \quad (8)$$

To solve Eq. (8) we require a model for the evolution of $F(l, l+1)$ and $F(l, l+2)$ which are correlation functions quantifying the degree to which the occupancy of the pairs of sites, $(l, l+1)$ and $(l, l+2)$, are correlated. To solve for these terms we consider the time rate of change of certain two-point distribution functions which are related to higher order distribution functions leading to an infinite system of equations that we close using the KSA [17,18]. For example, the evolution of $\rho^{(2)}(C_l, C_{l+1})$ is given by

$$\begin{aligned} \frac{d\rho^{(2)}(C_l, C_{l+1})}{dt} = & \frac{1}{2}[\rho^{(4)}(0_{l-2}, C_{l-1}, 0_l, C_{l+1}) + (1-\sigma)\rho^{(4)}(C_{l-2}, C_{l-1}, 0_l, C_{l+1})] + \frac{1}{2}[\rho^{(4)}(C_l, 0_{l+1}, C_{l+2}, 0_{l+3}) \\ & + (1-\sigma)\rho^{(4)}(C_l, 0_{l+1}, C_{l+2}, 0_{l+3})] - \frac{1}{2}[(1-\sigma)\rho^{(3)}(0_{l-1}, C_l, C_{l+1}) + (1-\sigma)\rho^{(3)}(C_l, C_{l+1}, 0_{l+2})]. \end{aligned} \quad (9)$$

To simplify Eq. (9) we apply a summation rule [17] to rewrite the unbiased $\rho^{(4)}$ terms as equivalent $\rho^{(3)}$ terms. Then, we use the summation rule again to write some of the resulting $\rho^{(3)}$ terms as equivalent expressions depending only on $\rho^{(2)}$ terms. This gives us

$$\begin{aligned} \frac{d\rho^{(2)}(C_l, C_{l+1})}{dt} = & \frac{1}{2}[\rho^{(2)}(C_{l-1}, C_{l+1}) + \rho^{(2)}(C_l, C_{l+2}) - 2\rho^{(2)}(C_l, C_{l+1})] - \frac{\sigma}{2}[\rho^{(4)}(C_{l-2}, C_{l-1}, 0_l, C_{l+1}) + \rho^{(4)}(C_l, 0_{l+1}, C_{l+2}, C_{l+3})] \\ & + \frac{\sigma}{2}[\rho^{(3)}(0_{l-1}, C_l, C_{l+1}) + \rho^{(3)}(C_l, C_{l+1}, 0_{l+2})]. \end{aligned} \quad (10)$$

We now use the KSA to reduce the $\rho^{(3)}$ and $\rho^{(4)}$ terms in Eq. (10). For the $\rho^{(4)}$ terms we use [24]

$$\rho^{(4)}(\phi_l, \phi_m, \phi_n, \phi_o) = \frac{\rho^{(3)}(\phi_l, \phi_m, \phi_n)\rho^{(3)}(\phi_l, \phi_m, \phi_o)\rho^{(3)}(\phi_l, \phi_n, \phi_o)\rho^{(3)}(\phi_m, \phi_n, \phi_o)\rho^{(1)}(\phi_l)\rho^{(1)}(\phi_m)\rho^{(1)}(\phi_n)\rho^{(1)}(\phi_o)}{\rho^{(2)}(\phi_l, \phi_m)\rho^{(2)}(\phi_l, \phi_n)\rho^{(2)}(\phi_l, \phi_o)\rho^{(2)}(\phi_m, \phi_n)\rho^{(2)}(\phi_m, \phi_o)\rho^{(2)}(\phi_n, \phi_o)}. \quad (11)$$

The $\rho^{(3)}$ terms appearing in Eq. (11) can then be reduced into $\rho^{(2)}$ terms using Eq. (7).

At this stage there are two possible ways to simplify Eq. (10). Either we

- (1) introduce the KSA directly into Eq. (10) to express the $\rho^{(3)}$ and $\rho^{(4)}$ terms as $\rho^{(2)}$ terms, or
- (2) apply the summation rule again to further simplify those terms in Eq. (10) that are proportional to σ .

Following the second approach we obtain

$$\begin{aligned} \frac{d\rho^{(2)}(C_l, C_{l+1})}{dt} = & \frac{1}{2}[\rho^{(2)}(C_{l-1}, C_{l+1}) + \rho^{(2)}(C_l, C_{l+2}) - 2\rho^{(2)}(C_l, C_{l+1})] - \frac{\sigma}{2}[\rho^{(2)}(C_{l-1}, C_{l+1}) + \rho^{(2)}(C_l, C_{l+2}) - 2\rho^{(2)}(C_l, C_{l+1})] \\ & + \frac{\sigma}{2}[\rho^{(4)}(0_{l-2}, C_{l-1}, 0_l, C_{l+1}) + \rho^{(4)}(C_l, 0_{l+1}, C_{l+2}, 0_{l+3})]. \end{aligned} \quad (12)$$

We apply the KSA to Eq. (12) and rewrite everything in terms of the correlation functions to obtain

$$\begin{aligned} \frac{dF(l, l+1)}{dt} = & -F(1, 1+1) \left[\frac{dc_{l+1}}{dt} \frac{1}{c_{l+1}} + \frac{dc_l}{dt} \frac{1}{c_l} \right] + \frac{1}{2} \left[\frac{c_{l-1}}{c_l} F(l-1, l+1) + \frac{c_{l+2}}{c_{l+1}} F(l, l+2) - 2F(l, l+1) \right] \\ & - \frac{\sigma}{2} \left[\frac{c_{l-1}}{c_l} F(l-1, l+1) + \frac{c_{l+2}}{c_{l+1}} F(l, l+2) - 2F(l, l+1) \right] \\ & + \frac{\sigma}{2} \left[\frac{c_{l-1}}{c_l(1-c_{l-2})^2(1-c_l)^2} F(l-1, l+1) [1 - c_{l-2} - c_l + c_l c_{l-2} F(l-2, l)] \right. \\ & \times [1 - c_{l-2} F(l-2, l-1)] [1 - c_{l-2} F(l-2, l+1)] [1 - c_l F(l-1, l)] [1 - c_l F(l, l+1)] \left. \right] \\ & + \frac{\sigma}{2} \left[\frac{c_{l+2}}{c_{l+1}(1-c_{l+1})^2(1-c_{l+3})^2} F(l, l+2) [1 - c_{l+1} - c_{l+3} + c_{l+1} c_{l+3} F(l+1, l+3)] \right. \\ & \times [1 - c_{l+1} F(l, l+1)] [1 - c_{l+3} F(l, l+3)] [1 - c_{l+1} F(l+1, l+2)] [1 - c_{l+3} F(l+2, l+3)] \left. \right]. \end{aligned} \quad (13)$$

162 To solve the moment closure model we use the same initial
 163 condition, $c(x,0)$, as in the discrete simulations and set the
 164 initial values of $F(l,m) \equiv 1$, for all $m = l+1, l+2, l+3, \dots$
 165 and for all all lattice sites l [18]. While it is possible, in
 166 principle, to solve $F(l,m)$ for all values of m to cover the
 167 periodic domain, it is more practical to solve a truncated
 168 system $F(l,m)$ for $m = l+1, l+2, \dots, M$ assuming that
 169 $F(l, M+1) \equiv 1$. We did this iteratively by solving for c_l ,
 170 $F(l, l+1)$ and setting $F(l, l+2) \equiv 1$, and then separately
 171 solving for c_l , $F(l, l+1)$, $F(l, l+2)$ and setting $F(l, l+3) \equiv$
 172 1 . These two approaches yielded results for $c(x,t)$ that were
 173 indistinguishable. Therefore, we take the simplest possible
 174 approach and report results corresponding to the solution of
 175 c_l and $F(l, l+1)$ with $F(l, l+2) \equiv 1$. We also remark that,
 176 as we pointed out earlier, it is possible to simplify Eq. (10)
 177 in an alternative way by applying the KSA directly to the $\rho^{(3)}$
 178 and $\rho^{(4)}$ terms in that equation without using the summation
 179 rule. For completeness, we also resolved all problems in this
 180 work using the alternative expression for $dF(l, l+1)/dt$ and
 181 found that both approaches yielded $c(x,t)$ profiles that were
 182 indistinguishable.

183 IV. RESULTS AND DISCUSSION

184 We consider a lattice with $1 \leq x \leq 1000$, and an initial
 185 distribution of agents given by

$$c(x,0) = \begin{cases} 0.1, & 1 \leq x < 480 \\ 1.0, & 481 \leq x \leq 520 \\ 0.1, & 521 < x \leq 1000. \end{cases} \quad (14)$$

186 Periodic boundary conditions are imposed, and simulations
 187 are performed for a range of σ including $(-1.00, -0.95,$
 188 $-0.90, \dots, 0.90, 0.95, 1.00)$. In each case we estimate the
 189 density profile using 1000 identically prepared realizations.
 190 Results in Figs. 2 and 3 are given at $t = 1000$ and $t = 5000$, re-
 191 spectively. Snapshots are shown for modest ($\sigma = 0.65$), strong
 192 ($\sigma = 0.80$), and extreme ($\sigma = 0.95$) adhesion. We show 20
 193 identically prepared realizations of the same stochastic process
 194 which illustrate the effects of adhesion since clustering occurs
 195 when adhesion dominates [Figs. 2(b) and 3(b)]. The density
 196 profiles in the central region of the lattice are compared with
 197 the solutions of Eqs. (2), (4), and (8). The numerical solution
 198 of Eq. (2) is obtained with a finite difference approximation
 199 with constant grid spacing δx and implicit Euler stepping with
 200 constant time steps δt [28]. Picard linearization, with absolute
 201 error tolerance ϵ , is used to solve the resulting nonlinear
 202 algebraic systems. The numerical solutions of Eqs. (4) and (8)
 203 are obtained using a fourth order Runge-Kutta method with
 204 constant time step δt [18]. All numerical results presented in
 205 this paper are obtained using values of δx , δt , and ϵ chosen
 206 to be sufficiently small so that the numerical results are grid
 207 independent.

208 For all cases of extreme ($\sigma = 0.95$) and strong ($\sigma = 0.80$)
 209 adhesion shown in Figs. 2 and 3, the solution of Eq. (2)
 210 is discontinuous [Figs. 2(d), 2(j), 3(d), and 3(j)]. These
 211 discontinuities are associated with $D(c)$ becoming negative for
 212 a region of c [10,11,29]. In this regime the pde fails to predict
 213 the discrete profiles which appear to be smooth. For modest
 214 ($\sigma = 0.65$) adhesion the solution of Eq. (2) remains smooth

215 since $D(c) > 0$ [Figs. 2(p) and 3(p)]. For modest adhesion
 216 the accuracy of Eq. (2) is much higher relative to the strong
 217 ($\sigma = 0.80$) and extreme ($\sigma = 0.95$) adhesion cases. Although
 218 Eq. (2) performs better for $\sigma = 0.65$, we still observe that
 219 Eq. (2) slightly overestimates the peak density at $t = 1000$
 220 [Fig. 2(p)].

221 When $D(c)$ becomes negative for a region of c , the solution
 222 of Eq. (2) is qualitatively different from the solution when
 223 $D(c)$ is always positive. When $D(c)$ is always positive,
 224 Eq. (2) is uniformly parabolic and satisfies the usual maximum
 225 principle. This means that the solution is bounded by the initial
 226 condition so that, in our case, $c(x,t) \leq 1$ for all $t > 0$ [29,30].
 227 Conversely, when $D(c)$ becomes negative for a region of c ,
 228 Eq. (2) is not uniformly parabolic and does not satisfy the
 229 usual maximum principle. This means that $c(x,t)$ may become
 230 greater than the initial condition as the profile evolves [Figs.
 231 2(d) and 3(d)]. Similar behavior has been observed previously
 232 in a different context. DiCarlo [31] used a nonlinear diffusion
 233 equation, called Richards' equation, to study fluid flow through
 234 a partially saturated porous medium. This previous work
 235 showed that the infiltration front was monotone and never
 236 increased above the long-term saturation level whenever the
 237 nonlinear diffusivity function was always positive. Similar to
 238 our results, DiCarlo showed that when the nonlinear diffusivity
 239 function contained a negative region, the infiltration front
 240 became nonmonotone, and the saturation level at the leading
 241 edge increased above the long-term saturation level meaning
 242 that the governing equation no longer satisfied the usual
 243 maximum principle.

244 Comparing the averaged discrete profiles and the solution
 245 of Eq. (4) indicates that this model predicts smooth profiles;
 246 however these profiles do not accurately predict the discrete
 247 density data for strong ($\sigma = 0.80$) and extreme ($\sigma = 0.95$)
 248 adhesion [Figs. 2(e), 2(k), 3(e), and 3(k)]. Alternatively, the
 249 solution of Eq. (8) predicts smooth profiles that are accurate,
 250 even for strong ($\sigma = 0.80$) and extreme ($\sigma = 0.95$) adhesion
 251 [Figs. 2(f), 2(l), 3(f), and 3(l)]. These results provide us with a
 252 qualitative indication of the relative roles of the assumptions
 253 underlying Eq. (2). We see that Eq. (4), without truncation,
 254 provides a modest improvement over Eq. (2), whereas Eq. (8),
 255 with no truncation or independence assumptions, provides a
 256 major improvement relative to Eq. (2). This indicates that
 257 the key assumption leading to the failure of Eq. (2) is the
 258 independence assumption.

259 The moment closure model Eq. (8) also provides us with
 260 a quantitative measure of the role of correlation effects
 261 through the correlation functions, shown in Figs. 2(s), 2(t),
 262 3(s), and 3(t). Our results show that $F(l, l+1)$ increases
 263 with σ , confirming that correlation effects increase with
 264 increasing adhesion, and we see that the continuum $F(l, l+1)$
 265 profiles predict the discrete values quite well at both $t = 1000$
 266 [Fig. 2(s)] and $t = 5000$ [Fig. 3(s)]. We also present discrete
 267 estimates of $F(l, l+2)$ [Figs. 2(t) and 3(t)] which are neglected
 268 in our moment closure results since we set $F(l, l+2) = 1$.
 269 Comparing profiles of $F(l, l+1)$ and $F(l, l+2)$ show that
 270 nearest neighbor correlation effects are more pronounced than
 271 next nearest neighbor correlation effects. Our neglect of next
 272 nearest neighbor correlation effects in the moment closure
 273 model appears reasonable given the quality of the match
 274 between the discrete data and the solution of Eq. (8).

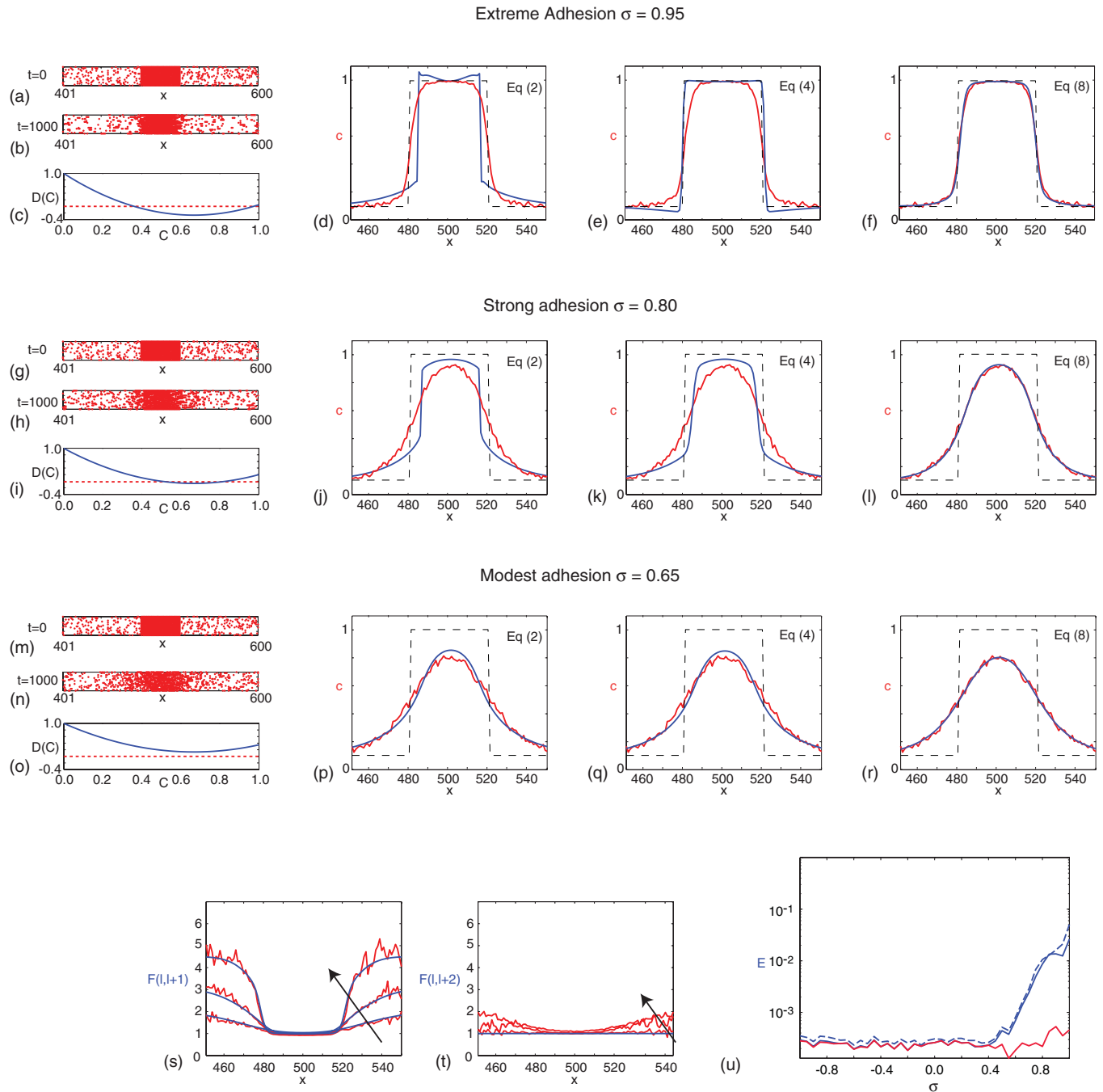


FIG. 2. (Color online) Mean-field and discrete results for a range of adhesive strengths: (a)–(f) extreme adhesion ($\sigma = 0.95$), (g)–(l) strong adhesion ($\sigma = 0.80$), and (m)–(r) modest adhesion ($\sigma = 0.65$). (a), (b); (g), (h); (m), (n) For each adhesive strength, two snapshots of the discrete process are shown at $t = 0$ and $t = 1000$, respectively. All discrete results correspond to $\Delta = \tau = 1$; simulations are performed on a lattice with $1 \leq x \leq 1000$ and periodic boundary conditions. Discrete snapshots show 20 identically prepared realizations of the same one-dimensional process in the region $401 \leq x \leq 600$. (d), (j), (p) Comparisons of averaged density profiles (red), the initial condition (black dashed), and the solution of Eq. (2) (blue). (e), (k), (q) Comparisons of averaged density profiles (red), the initial condition (black dashed), and the solution of Eq. (4) (blue). (f), (l), (r) Comparisons of averaged density profiles (red), the initial condition (black dashed), and the solution of Eq. (8) (blue). All discrete simulation results and mean-field solutions were obtained using periodic boundary conditions. (c), (i), (o) Show the nonlinear diffusivity function, $D(c) = 1 - \sigma c(4 - 3c)$, associated with Eq. (2). Results for extreme ($\sigma = 0.95$) and strong ($\sigma = 0.80$) adhesion show that $D(c)$ becomes negative in some interval $c \in [c_1, c_2]$ while results for the modest adhesion ($\sigma = 0.65$) show that $D(c) > 0$ for all $c \in [0, 1]$. (s), (t) Continuum (blue) and discrete (red) profiles of $F(l, l + 1)$ and $F(l, l + 2)$, respectively. In each plot, profiles of the correlation function are given for extreme ($\sigma = 0.95$), strong ($\sigma = 0.80$), and modest adhesion ($\sigma = 0.65$) with the arrow showing the direction of increasing σ . (u) The error profile E as a function of the adhesion parameter $\sigma \in [-1, 1]$ at $t = 1000$. Error profiles are given for Eqs. (2) (blue dashed), (4) (blue), and (8) (red). All numerical solutions of Eq. (2) correspond to $\delta x = 0.2$, $\delta t = 0.01$ and $\epsilon = 1 \times 10^{-6}$. All numerical solutions of Eqs. (4) and (8) correspond to $\delta t = 0.05$.

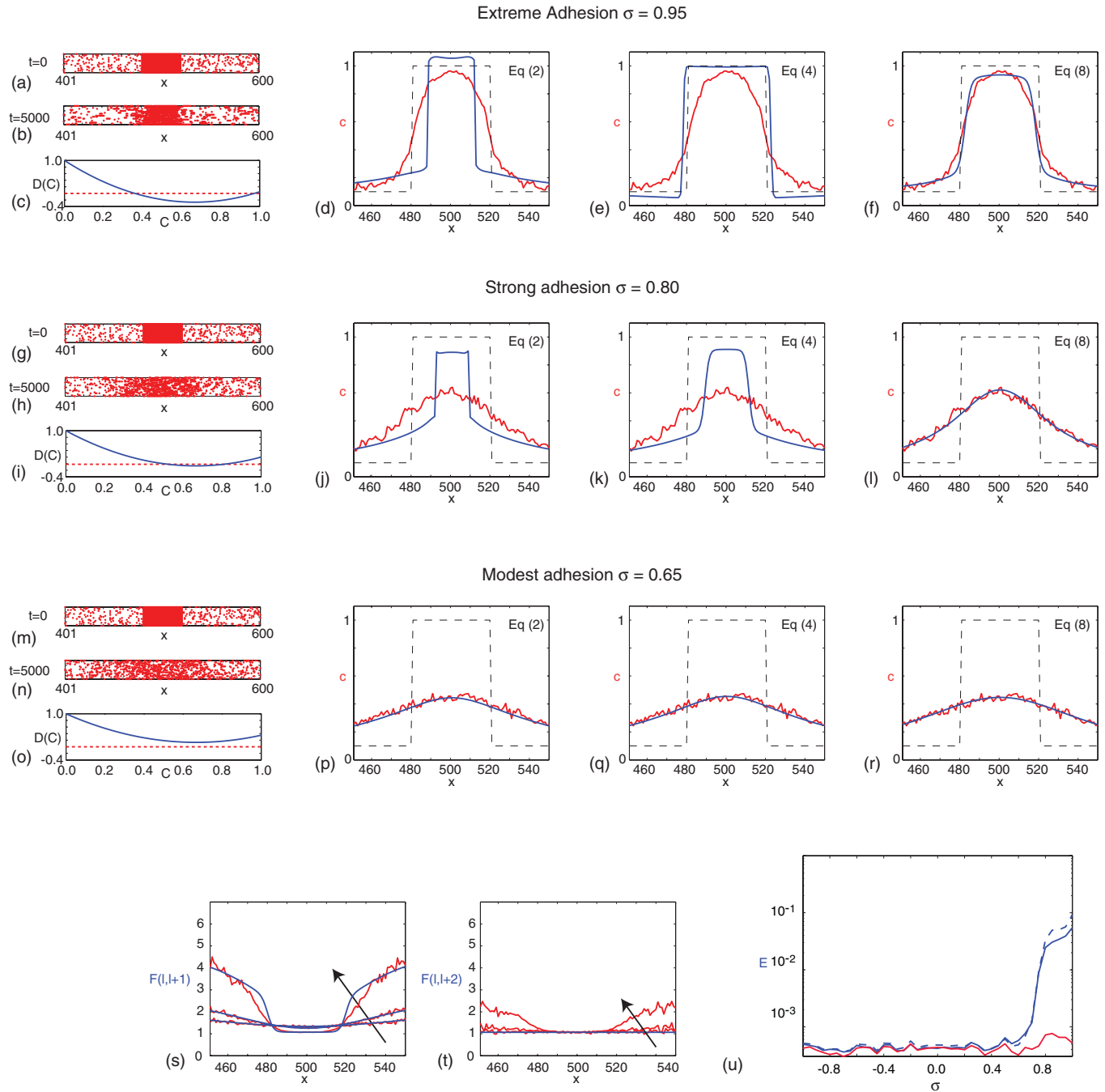


FIG. 3. (Color online) Mean-field and discrete results for a range of adhesive strengths: (a)–(f) extreme adhesion ($\sigma = 0.95$), (g)–(l) strong adhesion ($\sigma = 0.80$), and (m)–(r) modest adhesion ($\sigma = 0.65$). (a), (b); (g), (h); (m), (n) For each adhesive strength, two snapshots of the discrete process are shown at $t = 0$ and $t = 5000$, respectively. All discrete results correspond to $\Delta = \tau = 1$; simulations are performed on a lattice with $1 \leq x \leq 1000$ and periodic boundary conditions. Discrete snapshots show 20 identically prepared realizations of the same one-dimensional process in the region $401 \leq x \leq 600$. (d), (j), (p) Comparisons of averaged density profiles (red), the initial condition (black dashed), and the solution of Eq. (2) (blue). (e), (k), (q) Comparisons of averaged density profiles (red), the initial condition (black dashed), and the solution of Eq. (4) (blue). (f), (l), (r) Comparisons of averaged density profiles (red), the initial condition (black dashed), and the solution of Eq. (8) (blue). All discrete simulation results and mean-field solutions were obtained using periodic boundary conditions. (c), (i), (o) Show the nonlinear diffusivity function, $D(c) = 1 - \sigma c(4 - 3c)$, associated with Eq. (2). Results for extreme ($\sigma = 0.95$) and strong ($\sigma = 0.80$) adhesion show that $D(c)$ becomes negative in some interval $c \in [c_1, c_2]$ while results for the modest adhesion ($\sigma = 0.65$) show that $D(c) > 0$ for all $c \in [0, 1]$. (s), (t) Continuum (blue) and discrete (red) profiles of $F(l, l + 1)$ and $F(l, l + 2)$, respectively. In each plot, profiles of the correlation function are given for extreme ($\sigma = 0.95$), strong ($\sigma = 0.80$), and modest adhesion ($\sigma = 0.65$) with the arrow showing the direction of increasing σ . (u) The error profile E as a function of the adhesion parameter $\sigma \in [-1, 1]$ at $t = 5000$. Error profiles are given for Eqs. (2) (blue dashed), (4) (blue), and (8) (red). All numerical solutions of Eq. (2) correspond to $\delta x = 0.2$, $\delta t = 0.01$, and $\epsilon = 1 \times 10^{-6}$. All numerical solutions of Eqs. (4) and (8) correspond to $\delta t = 0.05$.

275 To quantify the accuracy of Eqs. (2), (4), and (8), we use
276 an error norm given by

$$E = \frac{1}{100} \sum_{l=451}^{l=550} [c_l - MF(x,t)]^2, \quad (15)$$

277 where $MF(x,t)$ is the density predicted by one of Eqs. (2)
278 and (4) or (8), and c_l is the average density at site l from
279 the averaged discrete simulations. We calculate E using sites
280 in the region $451 \leq l \leq 550$ since the details of the evolved
281 density profiles in Figs. 2 and 3 are localized in this region.
282 Figures 2(u) and 3(u) compare the accuracy of Eqs. (2), (4), and
283 (8) for the entire range of the adhesion parameter $\sigma \in [-1, 1]$,
284 showing that the error varies over two orders of magnitude.
285 For all cases of repulsive motion ($\sigma < 0$) and mildly adhesive
286 motion ($0 < \sigma < 0.5$), Eqs. (2), (4), and (8) perform similarly;
287 we see that the solution of each mean-field model accurately
288 matches the discrete profiles. This is consistent with
289 previous research [11]. For modest to extreme adhesion
290 ($0.50 \leq \sigma \leq 1.0$), Eqs. (2) and (4) become very inaccurate,
291 while Eq. (8) continues to make accurate predictions for all
292 $\sigma \in [-1, 1]$.

293 Comparing the performance of Eqs (2), (4), and (8) in
294 Fig. 2 at $t = 1000$ with the results in Fig. 3 at $t = 5000$
295 indicates that the same qualitative trends are apparent at both
296 time points. The profiles at $t = 1000$ (Fig. 2) for extreme
297 adhesion ($\sigma = 0.95$) and strong adhesion ($\sigma = 0.80$) show
298 that the density profiles have not changed much from the
299 initial distribution, while the results for moderate adhesion
300 ($\sigma = 0.65$) show that the density profile has spread out much
301 further along the lattice by $t = 1000$. The profiles at $t = 5000$
302 (Fig. 3) for strong adhesion ($\sigma = 0.80$) show that the density
303 profile has spread much further across the lattice, and the
304 results for moderate adhesion ($\sigma = 0.65$) show that the density
305 profile is almost horizontal by $t = 5000$. Since our work
306 is motivated by studying cell migration assays, which are
307 typically conducted over relatively short time periods, it is
308 appropriate for us to focus on relatively short simulations so
309 that we can examine the transient response of the system and
310 investigate how the shape of the initial condition changes.
311 Our results for extreme adhesion ($\sigma = 0.95$) indicate that
312 these profiles do not change much during the timescale of
313 the simulations whereas our results for strong ($\sigma = 0.80$) and
314 moderate ($\sigma = 0.65$) adhesion show that the profiles change
315 dramatically during the timescale of the simulations. It is
316 important that we consider this range of behaviors since similar
317 observations are often made in cell migration experiments
318 where certain cell types do not migrate very far over some time
319 periods, whereas other cell types migrate over much larger
320 distances during the same time period [32]. One hypothesis
321 that might explain these experimental results is that certain
322 cell types are affected by cell-to-cell adhesion much more than
323 other cell types [32]. The key result of our work is to show
324 that the usual mean-field model, given by Eq. (2), is unable
325 to describe the discrete data for strong and extreme adhesion
326 at any time point. This is significant because many previous
327 studies have derived traditional mean-field pde models which
328 suffer from the same limitations as Eq. (2). None of these
329 previous studies have presented any alternative mean-field

models that can predict the averaged discrete profiles when
contact effects dominate [6,8,11,12,14].

330 Although all density profiles shown in Figs. 2 and 3
331 correspond to adhesion ($\sigma > 0$), we also generated similar
332 profiles over the entire range of the parameter $\sigma \in [-1, 1]$
333 to obtain the error profile in Figs. 2(u) and 3(u). Results for
334 $\sigma < 0$ correspond to agent repulsion [11], and the contact
335 effects act to increase the rate at which the density profile
336 smooths with time. In this context, results with $\sigma < 0$ are less
337 interesting since $D(c)$ is always positive and agent clustering
338 does not occur. Furthermore, Eq. (2) appears to make accurate
339 predictions for all cases of repulsion. Therefore, we choose to
340 present snapshots and detailed comparisons in Figs. 2 and 3
341 for adhesion cases only ($\sigma > 0$).
342
343

344 Our comparisons of Eqs (2), (4), and (8) in Figs. 2 and 3
345 were for an initial condition Eq. (14) where the average
346 occupancy of sites was either $c(x,0) = 0.1$ or $c(x,0) = 1.0$
347 with a sharp discontinuity between these two values. We
348 chose this initial condition because Eq. (2) is well posed
349 since the initial condition jumps across the region where
350 $D(c)$ is negative. With $\sigma > 0.75$, $D(c)$ in Eq. (2) contains
351 a region $c \in [c_1, c_2]$ where $D(c) < 0$ ($0 < c_1 < c_2 < 1$), and
352 it is only possible to solve Eq. (2) when the initial condition
353 is chosen such that $c(x,0)$ is not in the interval $[c_1, c_2]$ [29].
354 Had we chosen an initial condition that did not obey these
355 restrictions, Eq. (2) would be ill posed with no solution [29].
356 For completeness, we now consider a second set of results for
357 a different initial condition given by

$$c(x,0) = 0.1 + 0.9 \exp \left[\frac{-(x-500)^2}{400} \right]. \quad (16)$$

358 This initial condition is Gaussian shaped and accesses all
359 values of $0.1 < c(x,0) < 1$. For values of $\sigma > 0.75$, this initial
360 condition does not jump across the region where $D(c)$ is
361 negative which means that Eq. (2) is ill posed, and we cannot
362 obtain a solution [13,29]. Regardless of this complication
363 with Eq. (2), we repeated all simulations shown previously
364 in Figs. 2 and 3 with the Gaussian-shaped initial condition,
365 and we report the results in Figs. 4 and 5 at $t = 1000$ and
366 $t = 5000$, respectively.

367 Results in Figs. 4 and 5 show the exact same qualitative
368 trends that were illustrated previously in Figs. 2 and 3. For
369 modest adhesion ($\sigma = 0.65$) we see that Eqs. (4) and (8)
370 perform similarly and both mean-field models predict the
371 averaged discrete data accurately [Figs. 4(n), 4(o), 5(n), and
372 5(o)]. For strong ($\sigma = 0.80$) and extreme adhesion ($\sigma = 0.85$),
373 we see that Eq. (4), which neglects correlation effects, is
374 unable to predict the averaged discrete data at either $t =$
375 1000 or $t = 5000$ [Figs. 4(d), 4(i), 5(d), and 5(i)] whereas
376 Eq. (8) leads to an accurate mean-field prediction in all cases
377 considered here. Comparing discrete estimates of $F(l, l+1)$
378 with those predicted using the moment closure model shows
379 that the moment closure approach captures nearest neighbor
380 correlation effects accurately [Figs. 4(p) and 5(p)], and we
381 see that next nearest neighbor correlation effects are less
382 pronounced than nearest neighbor correlation effects. The
383 differences in the performance of Eqs. (4) and (8) are quantified
384 in terms of the error norm Eq. (15) in Figs. 4(r) and 5(r).

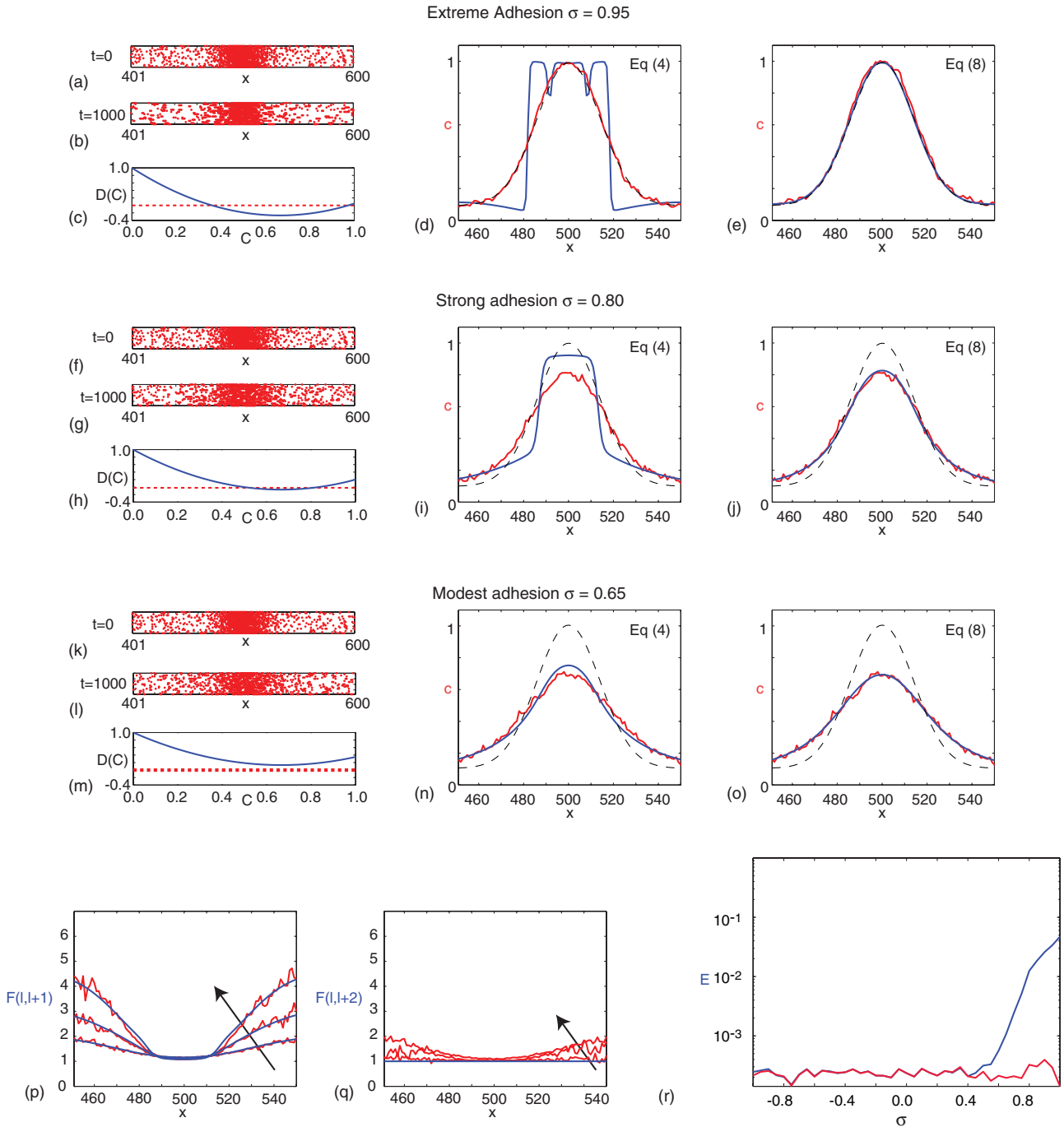


FIG. 4. (Color online) Mean-field and discrete results for a range of adhesive strengths: (a)–(e) extreme adhesion ($\sigma = 0.95$), (f)–(j) strong adhesion ($\sigma = 0.80$), and (k)–(o) modest adhesion ($\sigma = 0.65$). (a), (b); (f), (g); (k), (l) For each adhesive strength, two snapshots of the discrete process are shown at $t = 0$ and $t = 1000$, respectively. All discrete results correspond to $\Delta = \tau = 1$; simulations are performed on a lattice with $1 \leq x \leq 1000$ and periodic boundary conditions. Discrete snapshots show 20 identically prepared realizations of the same one-dimensional process in the region $401 \leq x \leq 600$. (d), (i), (n) Comparisons of averaged density profiles (red), the initial condition (black dashed), and the solution of Eq. (4) (blue). (e), (j), (o) Comparisons of averaged density profiles (red), the initial condition (black dashed), and the solution of Eq. (8) (blue). All discrete simulation results and mean-field solutions were obtained using periodic boundary conditions. (c), (h), (m) show the nonlinear diffusivity function, $D(c) = 1 - \sigma c(4 - 3c)$, associated with Eq. (2). Results for extreme ($\sigma = 0.95$) and strong ($\sigma = 0.80$) adhesion show that $D(c)$ becomes negative in some interval $c \in [c_1, c_2]$ while results for the modest adhesion ($\sigma = 0.65$) show that $D(c) > 0$ for all $c \in [0, 1]$. (p), (q) Continuum (blue) and discrete (red) profiles of $F(l, l + 1)$ and $F(l, l + 2)$, respectively. In each plot, profiles of the correlation function are given for extreme ($\sigma = 0.95$), strong ($\sigma = 0.80$), and modest adhesion ($\sigma = 0.65$) with the arrow showing the direction of increasing σ . (r) The error profile E as a function of the adhesion parameter $\sigma \in [-1, 1]$ at $t = 1000$. Error profiles are given for Eqs. (4) (blue) and (8) (red). All numerical solutions of Eq. (2) correspond to $\delta x = 0.2$, $\delta t = 0.01$, and $\epsilon = 1 \times 10^{-6}$. All numerical solutions of Eqs. (4) and (8) correspond to $\delta t = 0.05$.

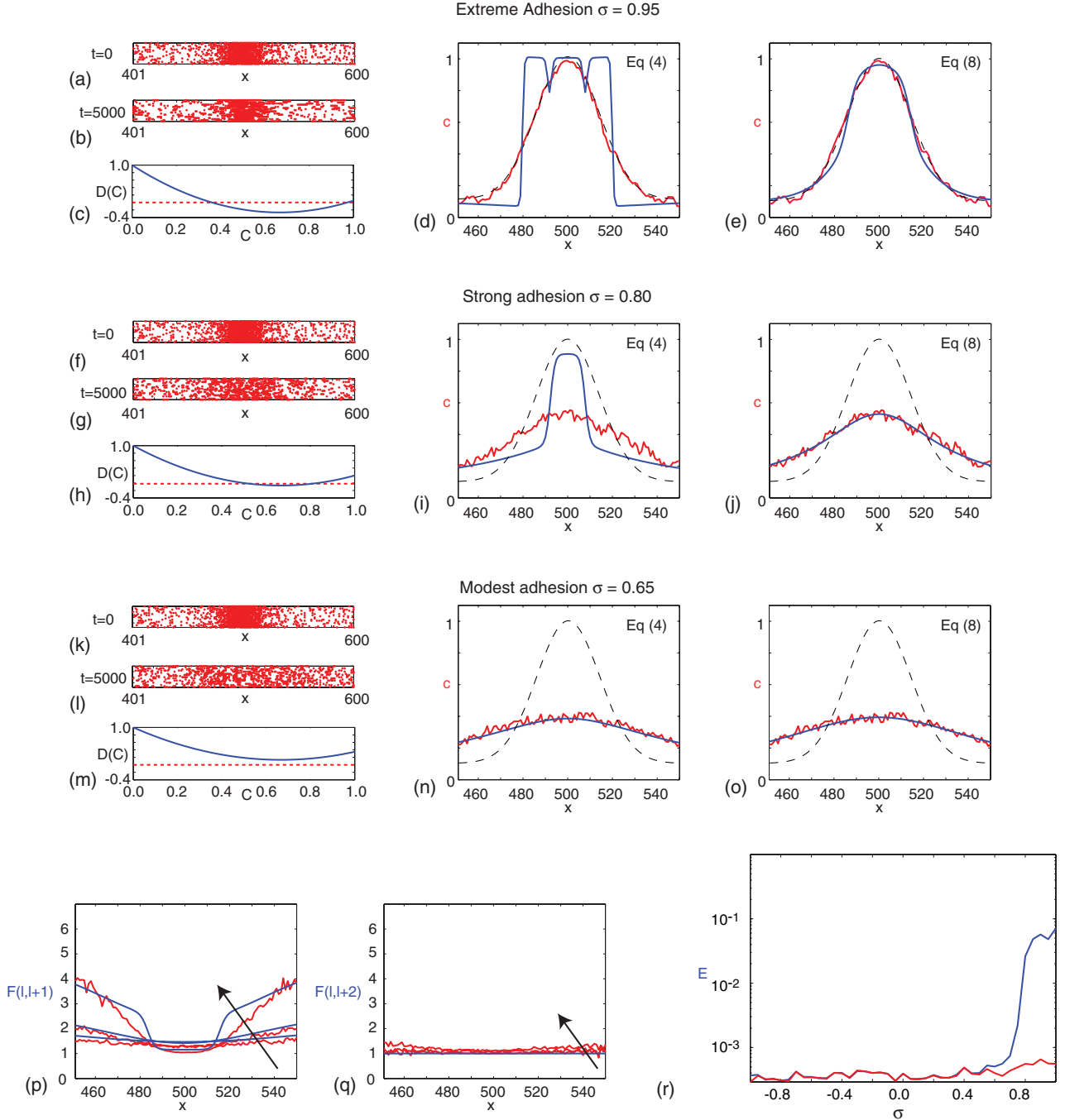


FIG. 5. (Color online) Mean-field and discrete results for a range of adhesive strengths: (a)–(e) extreme adhesion ($\sigma = 0.95$), (f)–(j) strong adhesion ($\sigma = 0.80$), and (k)–(o) modest adhesion ($\sigma = 0.65$). (a), (b); (f), (g); (k), (l) For each adhesive strength, two snapshots of the discrete process are shown at $t = 0$ and $t = 5000$, respectively. All discrete results correspond to $\Delta = \tau = 1$; simulations are performed on a lattice with $1 \leq x \leq 1000$ and periodic boundary conditions. Discrete snapshots show 20 identically prepared realizations of the same one-dimensional process in the region $401 \leq x \leq 600$. (d), (i), (n) Comparisons of averaged density profiles (red), the initial condition (black dashed), and the solution of Eq. (4) (blue). (e), (j), (o) Comparisons of averaged density profiles (red), the initial condition (black dashed), and the solution of Eq. (8) (blue). All discrete simulation results and mean-field solutions were obtained using periodic boundary conditions. (c), (h), (m) Show the nonlinear diffusivity function, $D(c) = 1 - \sigma c(4 - 3c)$, associated with Eq. (2). Results for extreme ($\sigma = 0.95$) and strong ($\sigma = 0.80$) adhesion show that $D(c)$ becomes negative in some interval $c \in [c_1, c_2]$ while results for the modest adhesion ($\sigma = 0.65$) show that $D(c) > 0$ for all $c \in [0, 1]$. (p), (q) Continuum (blue) and discrete (red) profiles of $F(l, l + 1)$ and $F(l, l + 2)$, respectively. In each plot, profiles of the correlation function are given for extreme ($\sigma = 0.95$), strong ($\sigma = 0.80$), and modest adhesion ($\sigma = 0.65$) with the arrow showing the direction of increasing σ . (r) The error profile E as a function of the adhesion parameter $\sigma \in [-1, 1]$ at $t = 5000$. Error profiles are given for Eqs. (4) (blue) and (8) (red). All numerical solutions of Eq. (2) correspond to $\delta x = 0.2$, $\delta t = 0.01$, and $\epsilon = 1 \times 10^{-6}$. All numerical solutions of Eqs. (4) and (8) correspond to $\delta t = 0.05$.

V. CONCLUSION

385
386 Our analysis shows it is possible to make accurate
387 mean-field predictions of a discrete exclusion process with
388 strong adhesion. Other mean-field predictions are valid for
389 mild contact effects only [6–8,11,12,14]. Identifying and
390 quantifying why traditional mean-field models fail to predict
391 highly adhesive motion requires new approaches that relax
392 the assumptions underlying the traditional approach. Our suite
393 of mean-field models allow us to quantify the accuracy of
394 assumptions relating to spatial truncation effects, and the
395 neglect of correlation effects. We find that the traditional pde
396 is extremely sensitive to the neglect of correlations.

397 The model presented in this paper is a simplified model of
398 cell migration since it deals only with one-dimensional motion
399 without cell birth and death processes. Our previous work on
400 moment closure models has shown how to incorporate cell

birth and death processes, as well as showing that it is possible 401
to develop moment closure models in higher dimensions. 402
These additional details could also be incorporated into 403
the current model. Other extensions to the discrete model 404
include studying adhesive migration where we explicitly 405
account for agent shape and size effects [33], or the study of 406
adhesive migration on a growing substrate [34]. We anticipate 407
that accurate mean-field models of these these extensions 408
will require a similar, but more detailed, moment closure 409
approach. 410

ACKNOWLEDGMENTS

We acknowledge support from Emeritus Professor Sean 412
McElwain, the Australian Research Council Project No. 413
DP0878011, and the Australian Mathematical Sciences 414
Institute for a summer vacation scholarship to S.T.J. 415

-
- [1] K. Kendall, *Molecular Adhesion and Its Applications* (Kluwer, New York, 2004).
- [2] *The Physics of Granular Media*, edited by Haye Hinrichsen and Dietrich E. Wolf (Wiley-VCH, Weinheim, 2006).
- [3] L. Wolpert, *Principles of Development* (Oxford University Press, Oxford, 2002).
- [4] R. A. Weinberg, *The Biology of Cancer* (Garland Science, New York, 2007).
- [5] T. M. Liggett, *Stochastic Interacting Systems: Contact, Voter and Exclusion Processes* (Springer, New York, 1999).
- [6] C. Deroulers, M. Aubert, M. Badoual, and B. Grammaticos. *Phys. Rev. E* **79**, 031917 (2009).
- [7] E. Khain, M. Katakowski, S. Hopkins, A. Szalad, X. Zheng, F. Jiang, and M. Chopp, *Phys. Rev. E* **83**, 031920 (2011).
- [8] M. J. Simpson, C. Towne, D. L. Sean McElwain, and Z. Upton, *Phys. Rev. E* **82**, 041901 (2010).
- [9] E. Khain, L. Sander, and C. M. Schneider-Mizell, *J. Stat. Phys.* **128**, 209 (2007).
- [10] K. Anguige and C. Schmeiser, *J. Math. Biol.* **58**, 395 (2009).
- [11] A. E. Fernando, K. A. Landman, and M. J. Simpson, *Phys. Rev. E* **81**, 011903 (2010).
- [12] C. J. Penington, B. D. Hughes, and K. A. Landman, *Phys. Rev. E* **84**, 041120 (2011).
- [13] M. J. Simpson, K. A. Landman, B. D. Hughes, and A. E. Fernando, *Physica A* **389**, 1412 (2010).
- [14] K. A. Landman and A. E. Fernando, *Physica A* **390**, 3742 (2011).
- [15] D. Chowdhury, S. Schadschneider, and K. Nishinari, *Phys. Life Rev.* **2**, 318 (2005).
- [16] E. A. Codling, M. J. Plank, and S. Benhamou, *J. R. Soc. Interface.* **5**, 813 (2008).
- [17] R. E. Baker and M. J. Simpson, *Phys. Rev. E* **82**, 041905 (2010).
- [18] M. J. Simpson and R. E. Baker, *Phys. Rev. E* **83**, 051922 (2011).
- [19] J. Mai, N. V. Kuzovkov, and W. von Niessen, *J. Chem. Phys.* **98**, 10017 (1993).
- [20] J. Mai, N. V. Kuzovkov, and W. von Niessen, *Physica A* **203**, 298 (1994).
- [21] R. Law, D. J. Murrell, and U. Dieckmann, *Ecology* **84**, 252 (2003).
- [22] D. J. Murrell, U. Dieckmann, and R. Law, *J. Theor. Biol.* **229**, 421 (2004).
- [23] M. Raghib, N. A. Hill, and U. Dieckmann, *J. Math. Biol.* **62**, 605 (2011).
- [24] A. Singer, *J. Chem. Phys.* **121**, 3657 (2004).
- [25] K. J. Sharkey, *J. Math. Biol.* **57**, 311 (2008).
- [26] C. E. Dangerfield, J. V. Ross, and M. J. Keeling, *J. R. Soc. Interface.* **6**, 761 (2009).
- [27] K. Seki and M. Tachiya, *Phys. Rev. E* **80**, 041120 (2009).
- [28] M. J. Simpson, K. A. Landman, and T. P. Clement, *Math. Comput. Simulat.* **70**, 44 (2005).
- [29] T. P. Witelski, *Appl. Math. Lett.* **8**, 27 (1995).
- [30] M. H. Protter and H. F. Weinberger, *Maximum Principles in Differential Equations* (Prentice-Hall, New Jersey, 1967).
- [31] D. A. DiCarlo, R. Juanes, T. LaForce, and T. P. Witelski, *Water Resour. Res.* **44**, W02406 (2008).
- [32] Y. Kam, C. Guess, L. Estrada, B. Weidow, and V. Quaranta, *BMC Cancer.* **8**, 198 (2008).
- [33] M. J. Simpson, R. E. Baker, and S. W. McCue, *Phys. Rev. E* **83**, 021901 (2011).
- [34] B. J. Binder, K. A. Landman, M. J. Simpson, M. Mariani, and D. F. Newgreen, *Phys. Rev. E* **78**, 031912 (2008).